RESEARCH PAPER

Effect of Solution Treatment on the Rollability of a Cu-Ni-Mn-Sn Alloy

Morteza Hadi[1], Omid Bayat[2,*], Hadi Karimi[3], Mohsen Sadeghi[3], Taghi Isfahani[1]

* *obayat@hut.ac.ir*

[1] Materials Engineering Group, Golpayegan College of Engineering, Isfahan University of Technology, Golpayegan, Iran
[2] Department of Metallurgy and Materials Engineering, Hamedan University of Technology, Hamedan, Iran
[3] Department of Materials Engineering, Malek-Ashtar University of Technology, Iran

Received: June 2021 **Revised: December 2021** **Accepted: January 2022**

DOI: 10.22068/ijmse.2266

Abstract: *In this research, the effect of initial microstructure and solution treatment on rollability and crystallographic texture of a Cu-Mn-Ni-Sn alloy has been investigated. The initial tests indicated that the rolling of the alloy at different temperature was not possible due to formation of second phases. Therefore, to eliminate the phase segregation, proper temperature for solution treatment was selected as 750°C using DTA data. The obtained results showed that after 15-hour solution treatment at this temperature, the complete elimination of Sn, Mn, Ni, and Fe-rich phases may be achieved. Also, XRD data showed shift of peaks to higher angles indicating that the alloying elements were dissolved in the structure. Meanwhile, the intensity of the texture reduced and the dominant texture changed from Goss and Brass-texture to Copper-texture. Accordingly, the amount of maximum total reduction at the rolling process increased from 16.37 to 109.46 after solution treatment.*

Keywords: *Microstructure, Texture, X-ray diffraction (XRD), rollability, Solution treatment.*

1. INTRODUCTION

The main parameters for selecting brazing alloys for the joining of the engineering parts are melting temperature and wettability of the filler material and strength, fracture toughness, and corrosion resistance of the joints [1, 2]. Apart from the unique physical properties of Cu, brazing alloys based on Cu-Ni-Mn are suitable candidates for the dissimilar joining of steel, especially stainless steel to the copper alloys [3-5]. In the past years, investigations have been performed to modify this three-constituent composition to improve brazing joints [6, 7]. One of the most important classes of brazing alloys in this system are Cu-Mn-Ni-Sn alloys and especially the grade of this system which contains Fe, Si, and B is known as PM17. This alloy is used for brazing Cu-Cr-Zr-Ti alloy to the steel parts [1, 8], brazing three-layer structure of high-strength steels [9], and the brazing of Cu-Cr-Zr bronze to SS321 [10]. Since the brazing process is based on the capillary attraction property, the filler of the brazing should be placed in the designed thin gap [1]. According to the published research, the PM17 brazing alloy has been used as filler brazing with a small thickness from 0.08 to 0.3 mm in the form of strips and foils [8-10]. Therefore, the rollability of this brazing alloy to reach a small thickness is very important. In the rollability studies, improvements were obtained by adding alloying elements or applying proper heat treatment [11-16]. The deformation of alloys containing Sn (similar to PM17 alloy) such as Cu-Sn [17, 18], Cu-Ni-Sn [19, 20], Cu-Zn-Sn [21] have been studied recently but up to our knowledge, there is no report on the rollability of this brazing alloy. Due to the high amount of alloying elements in the alloy with a nominal composition of Cu-(15-17)Mn-(12.5-14)Ni-(5-6) Sn-(0-1-2) Fe-(0.2-0.6) Si-(0.15-0.3)B (%wt), [10] which could remarkably have affected formability, the study on the rolling process of this alloy is substantial for developing its application in dissimilar joining. In this investigation, improving the rollability of PM17 alloy with the help of special heat treatment was examined by microstructural, thermal, and texture studies as well as applying experimental rolling tests.

2. EXPERIMENTAL PROCEDURES

PM17 alloy according to nominal composition (Cu-17Mn-13Ni-5.5Sn-1.5Fe-0.4Si-0.2B (%Wt)) was prepared by vacuum induction melting furnace using pure charge materials. A vacuum of $5*10^{-3}$ mbar was followed by melting under a high purity Argon atmosphere at a pressure of

[Downloaded from stdc.iust.ac.ir on 2025-07-19]

[DOI: 10.22068/ijmse.2266]

800 mbar. Positive pressure was used to reduce manganese evaporation [22]. Both as-cast and solution treated specimens were rolled by a plate mill with rolls 350 mm and 100 mm in diameter. Different rolling temperatures of 25°C, 380°C, 480°C, 570°C, and 670°C were applied to the samples. Solution treatments were performed at 750°C for 1, 5, 10, 15, and 20 hours under Argon atmosphere. To achieve low thickness in the solution treated samples, a four-high rolling mill with 100 mm working rollers was used. The thermal transitions of the alloy were studied using NETZSCH STA 409 differential thermal analyzer at a heating rate of 10°C/min. Characterization of the specimens was done by X-ray diffraction (XRD) in a Seifert 3003TT diffractometer using Cu Kα radiation. The X-ray macrotexture analysis was performed by Asenware XDM300. The microstructures of the specimens were also studied by a field emission scanning electron microscope (FE-SEM MIRA TESCAN) equipped with an energy-dispersive spectrometer (EDS). ProCAST 2012 software was utilized to simulate the variations of solid fraction versus temperature.

3. RESULTS AND DISCUSSIONS

3.1. Phase evolution and microstructure

In order to investigate the rollability of the PM17 alloy, different rolling temperatures were applied to the as-cast samples. These temperatures were used to cover the cold, warm and hot working temperature range. Interestingly, in all of the rolled specimens, fracture occurred at the first step of the rolling. This fracture also occurred after applying the minimum possible reduction per pass (0.5 mm). The longitudinal cracks (which could be also considered as long tears) occurred in the samples suggesting that the reason for this failure might be microstructural problems. In order to determine the mode of fracture, the fracture surfaces of the specimens were studied by optical and scanning electron microscopes. A dendritic structure and microvoids between the dendrite arms as a result of the solidification process were distinguished in the fracture surface (Fig. 1). This microstructure was expectable due to the solidification of alloy with several alloying elements. In fact, hot work processes are typically used to remove such a dendrite structure. However, due to the fact that the hot rolling of the as-cast specimen also led to cracks, the possibility of microstructural segregation was considered for low workability. Although the bulk composition of the alloy was controlled by EDS, the large number and difference of atomic radius and melting temperature of alloying elements can cause compositional segregation. Therefore, for more details, the microstructure of as-cast alloy was studied by FE-SEM.

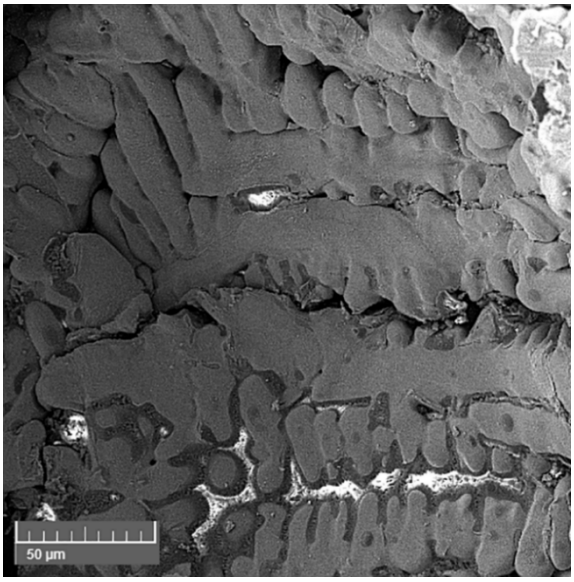

Fig. 1. Topography image from the fractured surface of the rolled as-cast specimen

Fig. 2 (a) and (b) show the microstructure of the as-cast alloy in two magnifications. The EDS analysis of the segregated phases denoted by A to D are presented in Table 1. Since the phases with different average atomic numbers in the composition have different contrasts in the BSE mode of SEM images, the presence of the four phases in addition to the matrix of the as-cast alloy was revealed by SEM investigations. As it is clear, the brightest phase (indicated by A) is rich in Sn which has the highest atomic number among the alloying elements. Also, this phase contains noticeable amounts of Mn and Ni elements. However, the phase indicated by B was a Cu-based phase and contained Sn more than the nominal composition of the alloy. Moreover, from the results of Table 1, the C and D zones were Ni-Mn and Fe-Mn rich phases, respectively. Finally, the EDS of the matrix is presented by E in Table 1.

[Downloaded from stdc.iust.ac.ir on 2025-07-19]

[DOI: 10.22068/ijmse.2266]

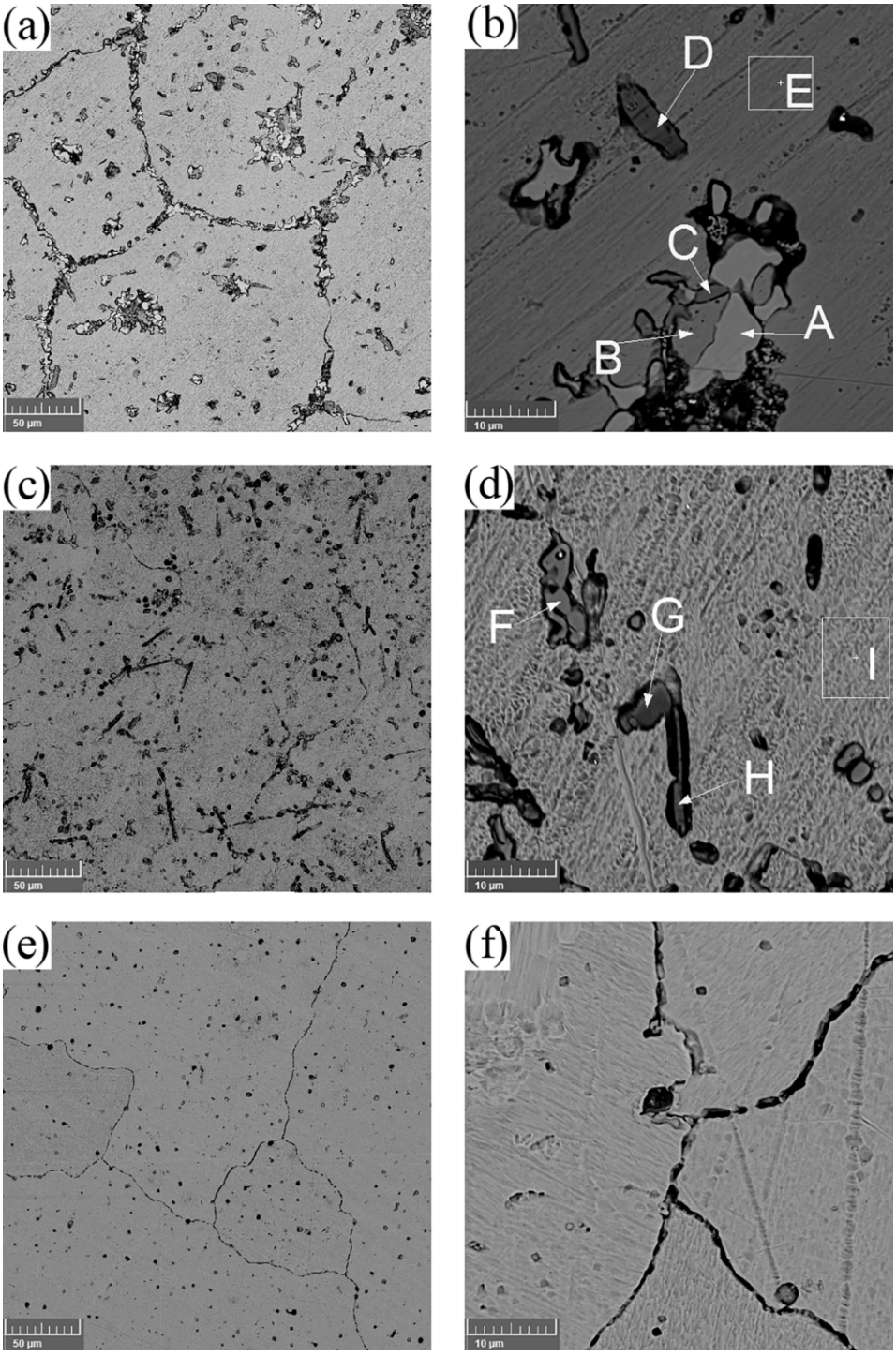

Fig. 2. Backscatter FE-SEM images of (a) and (b) as-cast, (c) and (d) solution treated sample at 750ºC for 10 h, (e) and (f) solution treated sample at 750ºC for 15 h

Table 1. The results of EDS analysis from segregated phases in as-cast alloy indicated in Fig 2 (b)

	Cu	Ni	Mn	Sn	Fe	Si
Point A	16.73	21.7	17.21	43.72	-	0.64
Point B	60.55	10.99	15.64	12.10	0.5	0.22
Point C	9.03	44.90	32.76	2.37	0.93	10.02
Point D	2.27	11.01	35.68	0.64	50.12	0.25
Point E	66.30	12.76	15.06	4.99	0.75	0.14

[Downloaded from stdc.iust.ac.ir on 2025-07-19]

[DOI: 10.22068/ijmse.2266]

3.2. Thermal analysis

Differential thermal analysis was used to determine the phase transition temperatures of the alloy. DTA result exhibited five endothermic peaks indicating the occurrence of phase transitions as can be seen in Fig. 3.

The last peak present in the DTA curve occurred at the temperature range of 850°C to 1000°C which can be attributed to the melting of the alloy. The extremum of this peak which shows the melting temperature of the alloy is equal to 960°C. The four other peaks might have been caused by solid-state phase transitions. The microstructural observations confirmed that the four peaks obtained from the DTA result might be attributed to the formation of the four segregated phases in the microstructure of the as-cast alloy (Fig. 2 (a) and (b)). There are some techniques for acquiring homogeneity during melting and casting of the alloys with different alloying elements such as using masteralloys and rapid solidification [23, 24] which were applied for PM17 alloying. However, segregation in the microstructure of the as-cast alloy was inevitable. To further clarify the phase transitions, the microstructure of the solution-treated specimens was studied. According to DTA curve, the temperature of 750°C which is higher than all four transition temperatures and lower than the melting range was selected. The observations of the heat-treated samples for 1, 5, 10, 15, and 20 hours made it clear that somehow the solution of the segregated phases occurred gradually and required a relativity long heat treatment time. Fig. 2 (c) and (d) represent the microstructure of the solution-treated alloy after 10 hours. From these figures, it is obvious that three segregated phases still remain in the microstructure of the alloy even after 10-hour solution treatment. From the EDS results, presented in Table 2, no more Sn-rich phases were detected in the microstructure. However, the first segregated zone denoted by F was identified as a Ni-rich phase.

It seems that this phase was formed due to the diffusion of the Mn and Sn atoms from phase C to the matrix in the as-cast microstructure after solution treatment. Similarly, complex and simultaneous diffusion of the alloying elements including iron, manganese, and nickel during solution treatment has been effective in the formation of new phases G and H. However, comparing Table 1 and 2 clearly confirmed that the solution treatment at 750°C for 10 hours was incomplete. Therefore, longer heat treatment was applied to the specimen.

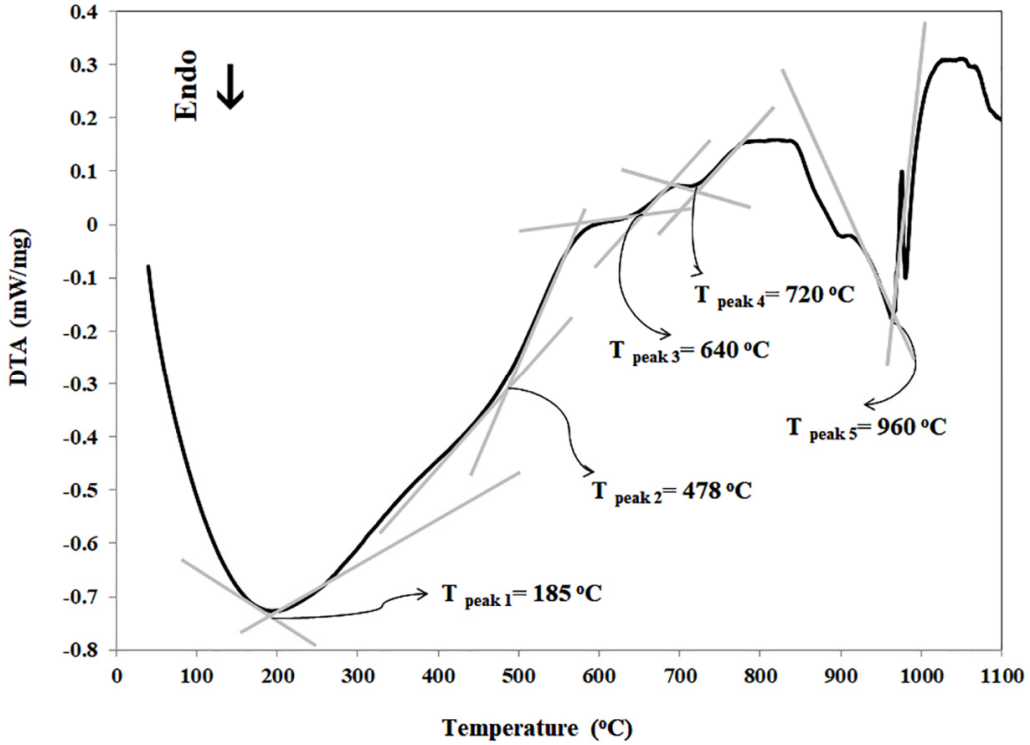

Fig. 3. DTA curve of the as-cast specimen obtained at a heating rate of 10°C/min

[Downloaded from stdc.iust.ac.ir on 2025-07-19]

[DOI: 10.22068/ijmse.2266]

Table 2. The EDS analysis results of the segregated phases in the solution treated alloy (at 850°C for 5 hours) as indicated in Fig 2 (d)

	Cu	Ni	Mn	Sn	Fe	Si
Point F	5.18	58.61	21.57	1.22	0.37	13.05
Point G	8.91	12.90	32.84	2.46	42.65	0.24
Point H	4.30	14.05	29.19	1.40	50.75	0.32
Point I	64.39	11.97	15.39	7.56	0.40	0.28

The microstructure of the 15-hour solution treated specimen is demonstrated in Fig. 2 (e) and (f). No more segregated phases were observed in the microstructure suggesting complete solution treatment after 15 hours. The scattered points in these images are clearly due to pitting corrosion created by the etching solution.

For an overall conclusion, the results of the FE-SEM and DTA images (Figs. 1 and 2) showed that in addition to the matrix, four segregated phases exist in the as-cast microstructure. The solution transformation of these phases showed endothermic peaks in the DTA curve. This could be attributed to the diffusion of Sn, Mn, and Ni atoms. According to the microstructure of the heat-treated specimens, the solution of the segregated phases is time-dependent and could be completed after 15 hours. Obviously, increasing the heat treatment time after complete solution treatment will not have a new effect on the microstructure, which was confirmed by a sample of 20 hours of heat treatment.

3.3. Crystalinity of the samples

In Fig. 4 the XRD patterns of the as-cast and 15-hour solution treated samples are presented. Segregated phases detected in the FE-SEM observations didn't show any peaks in the XRD pattern of the as-cast alloy. It can be interpreted as low amount of segregated phases in the microstructure of as-cast specimen (Fig. 2 (a)) which were not enough to be detectable in the XRD analysis. In addition, EDS analysis of the matrix of the alloy (point E in Table 1) was very close to the nominal composition of the alloy suggesting that the segregation didn't deviate the matrix composition, remarkably. Moreover, according to the atomic radius of the base elements of Cu, Ni, Mn, and Sn which are 1.28, 1.24, 1.26, and 1.62 Å, respectively and also by considering the large difference between the atomic radius of Sn and Cu; it seems that this element had the key role in reducing the diffraction angles of the as-cast alloy compared to pure copper. In fact, having a solution or compound with the Sn element which has a larger atomic radius resulted in the increase of the distance of the crystallography planes (d) and therefore the diffraction angles (2θ) of the as-cast alloy shifted to the left compared to pure copper (dashed lines). On the other hand, in the solution treated sample, with the solution of other elements such as Mn and Ni which have smaller atomic radius compared to the base metal, the distance of the crystallographic planes (d) reduced and as a result, the diffraction angles (2θ) of the solution treated sample slightly increased compared to the as-cast sample. Accordingly, the peaks of the solution treated specimen got closer to the diffraction angles of copper.

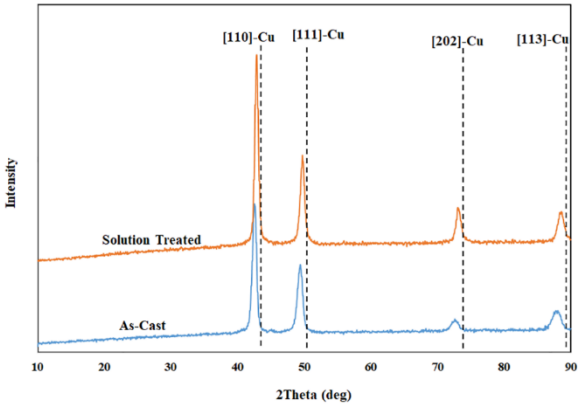

Fig. 4. XRD patterns of as-cast and 15-hour solution treated specimens. Diffraction angles of standard pattern 00-001-1241 corresponding to pure copper are shown as dashed lines

3.4. Texture investigation

The results of texture analysis on the as-cast and solution treated specimens after one-pass rolling (15% strain) are demonstrated in Fig. 5 and 6. Applying more strain to the as-cast specimen, as will be explained later, would cause cracks. For each sample, four pole figures were measured. The orientation distribution functions (ODF) were calculated from this data (Fig. 5) and then recalculated pole figures were obtained from

[Downloaded from stdc.iust.ac.ir on 2025-07-19]

[DOI: 10.22068/ijmse.2266]

ODF (Fig. 6). In General, reducing the intensity of overall texture in the solution treated specimen compared with the as-cast sample can be deduced from the ODFs and pole figures. In FCC metals, by considering whole Euler space and typical texture fiber, usually three angles of φ_2 including 0°, 45°, and 65 have been used for the texture analysis [25-27].

It should be noted that due to the crystalline symmetries in the FCC metals, section of 90° is similar to 0°. The high magnification images of these angles are also shown in Fig. 5. As can be seen, reducing brass-Texture {110}<112> and Goss texture {011}<110> and increasing copper-texture {112}<111> in solution treated specimen can be distinguished from the 0° and 45° images. Also, a slight decrease in the S-texture observed in 65° section. Meanwhile, comparing pole figures of {111}, it can be inferred that the intensity of Goss and Brass-textures decrease as solution treatment occurred (Fig. 6). However, the intensity of S and Cu-textures increased. Again, in {220}-pole figures, it can be seen particularly from the center of pole figure, where is the indication place for Goss- and Brass- texture, the intensity of these textures decreased after solution treatment. In fact, Knowing that copper element has high stacking fault energy (SFE), the texture of the as-cast alloy shows features of FCC metal which its SFE reduces by adding alloying elements. The results showed that the texture of as-cast alloy is more similar to transition texture from pure metal to alloy texture. However, after solution treatment, the feature of texture is more similar to the texture of high SFE pure metals. It seems by the solution of alloying elements in the matrix of the alloy, the {111} pole figure of the specimen becomes more like pure FCC metals. The changes of pole figures by adding elements to an FCC metal have been discussed elsewhere [26, 28]. This is consistent with the ODF results showing reduction of the intensity of Brass-fiber and increasing that of Cu-fiber occurred simultaneously after solution treatment. In the FCC metals with lower SFE, It has been found that the copper-oriented grains rotated around the <110> crystallographic axis and develop Brass and Goss texture [27].

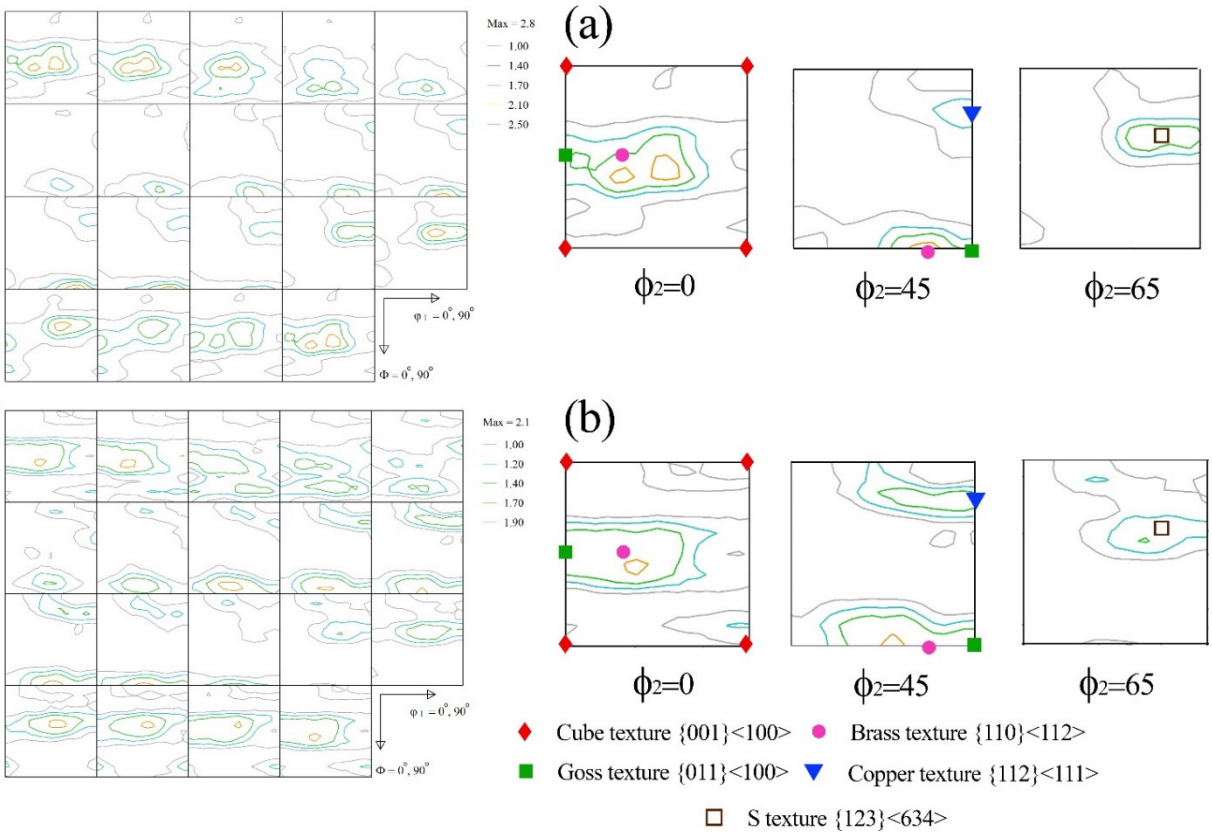

Fig. 5. ODF images of (a) as-cast and (b) solution treated specimens where the sections related to the three important angles in FFC metals are presented with higher magnification. This image also shows the location of typical texture fibers in FCC metals

[Downloaded from stdc.iust.ac.ir on 2025-07-19]

[DOI: 10.22068/ijmse.2266]

Also, it is worth mentioning that the ODF patterns of solution treated specimens in all three angles are more similar to typical patterns developed in the rolled copper foils [25].

The importance of the obtained results is due to the fact that many studies show the effect of solution treatment and crystalline texture modification on rollability [29-31]. In order to evaluate the rollability after the solution treatment procedure, the solution-treated samples were rolled at various temperatures. Observations showed that the longitudinal cracks occurred in the warm and hot working procedure which was similar to the as-cast specimens. However, relatively high reductions (for example 7 to 2 mm in thickness) could be achieved by rolling at room temperature without any cracks. Modification of microstructure by heat treatment to improve rollability was reported in previous work on other alloys [28, 32-35].

The rolling data of the as-cast and solution treated alloys for the cold and hot working procedures are presented in Tables 3. As can be concluded from this table, although a failure in the as-cast specimens occurs after two rolling passes, the solution treated samples could be rolled for up to seven passes at room temperature. Moreover, further reduction to produce a metal foil with a very fine thickness (e.g. 0.1 mm) using a four-high rolling mill is possible by intermediate annealing in the solution treated samples. Nevertheless, the results of rolling at 670°C revealed that even after solution treatment, hot rolling of the alloy is impossible. For a better evaluation of the rollability, the maximum total reduction (MTR) and maximum reduction per pass (MRPRP) were compared in Fig. 7. As can be seen, although the MTR of the as-cast specimen is 16%, it is about 109% for the solution-treated sample. Meanwhile, twice the amount of MRPRP could be achieved in the solution treated specimen at room temperature.

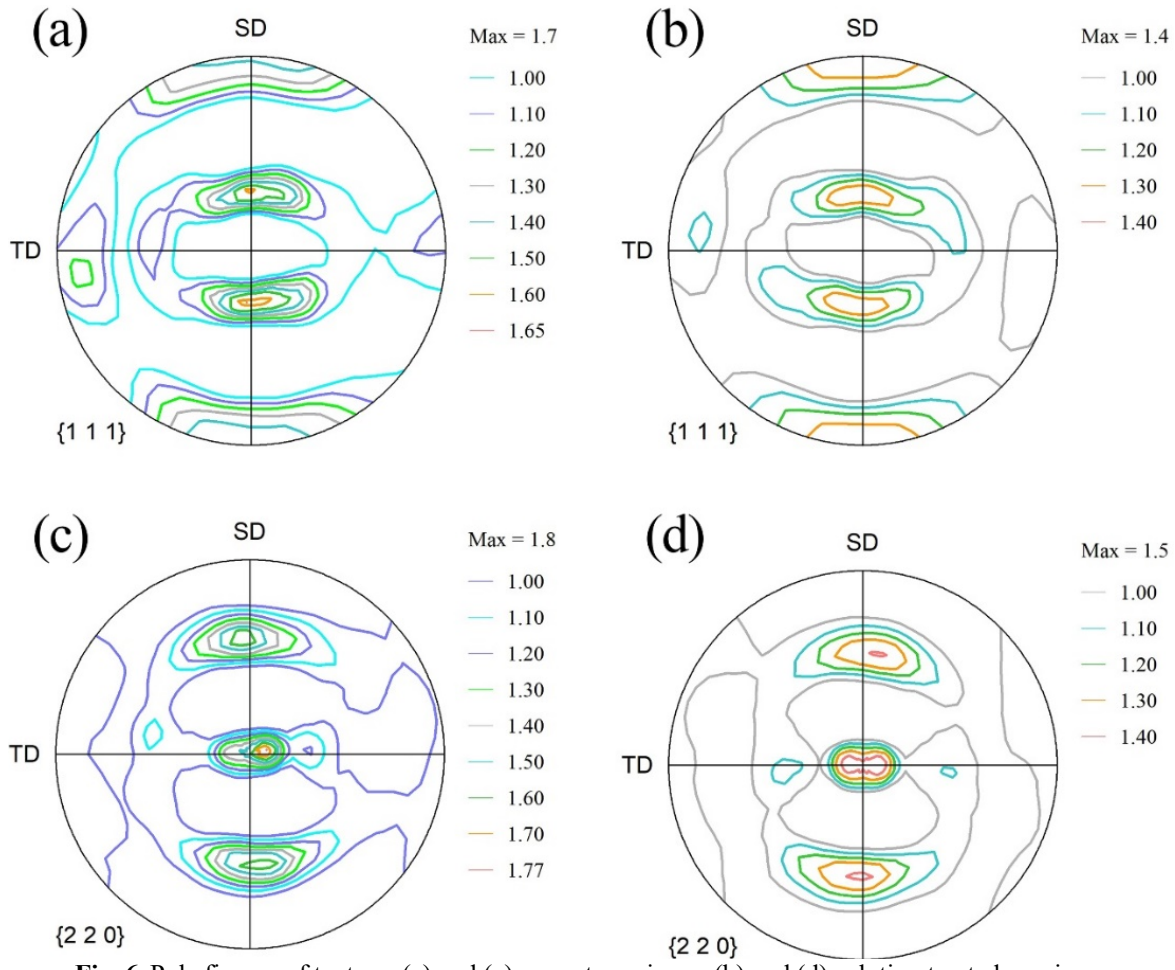

Fig. 6. Pole figures of texture: (a) and (c) as-cast specimen; (b) and (d) solution treated specimen

[Downloaded from stdc.iust.ac.ir on 2025-07-19]

[DOI: 10.22068/ijmse.2266]

Table 3. The rolling data obtained from the as-cast and solution treated alloy rolled at at room temperature and 670°C

Condition	pass number	initial thickness	final thickness	True strain	Eng Strain (%)	Strain rate
As-cast (RT)	1	7	6.5	0.07	7.14	1.45
	2	6.5	5.9	0.10	9.23	1.73
	3	5.9	Failure	-	-	-
Solution treated (RT)	1	7	6.4	0.09	8.6	1.6
	2	6.4	5.7	0.12	10.9	1.9
	3	5.7	4.8	0.17	15.8	2.5
	4	4.8	4	0.18	16.7	2.8
	5	4	3.2	0.22	20	3.5
	6	3.2	2.4	0.28	25	4.5
	7	2.4	2.1	0.13	12.5	3.4
As-cast (670°C)	1	7	Failure	-	-	-
Solution treated (670°C)	1	7	6.3	0.10	10	1.75
	2	6.3	5.1	0.21	19.04	2.67
	3	5.1	Failure	-	-	-

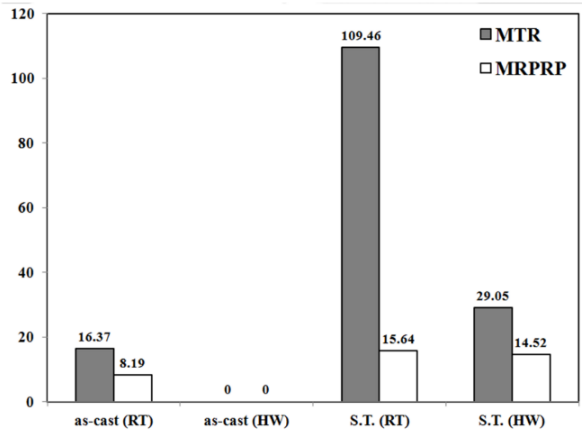

Fig. 7. The values of maximum total reduction (MTR) and maximum reduction per pass (MRPRP) in the as-cast and solution treated specimens (S.T.) at room temperature (RT) and hot working conditions (HW) with some related real pictures of the specimens.

On the other hand, hot rollability was not improved remarkably even after solution treatment. To ensure that the hot workability of the alloy was not affected by the apparatus parameters of the hot rolling process, a standard tension test at 670°C was performed on the solution-treated specimen.

The result showed the elongation of the alloy is very low at this temperature confirming the poor workability observed in the hot rolling process. To interpret the rolling results, it must be considered that the rollability of the alloy was significantly improved in the solution-treated samples (Fig. 7 and Table 3). This originates from the fact that in the multi-phase microstructure, the segregated phases with various hardness and formability could not be elongated uniformly along the rolling direction. Therefore, non-uniform distribution of strain and strain rate could be created which can cause instability in the rolling sample. Accordingly, cracks could be nucleated and progressed around the segregated phases, especially at the softer phases such as the Sn-rich phase. It has been found that the second phases according to their mean size, distribution, and hardness act as strengthening factors [36-38] and workability reducing factors [39]. Similar explanations about the effect of the second phase on the rollability of the AZ31 alloy were reported in the previous research [13]. Meanwhile, reducing the intensity of texture and changing dominant texture from Brass and Goss-Fibers to Cu-fiber led to improve rollability after solution treatment. Therefore, the increase of the MTR and MRPRP in the 15-hour solution treated specimens (Table 3 and Fig. 7) could be interpreted by preventing the deformation instability. Conversely, the capability of the hot rolling was not noticeably improved even after the 15-hour solution treatment (Table 3 and Fig. 7). In order to get a deeper insight into the reasons for the cracking during the hot working, state changes of the alloy were simulated by Pro-CAST software. The estimation of the solid volume fraction versus the temperature showed that even at 500°C the fraction of the solid is lower than 1. Therefore, the presence of the liquid phase in the microstructure is a possible explanation for the nucleation of the cracks during hot working. Even though the

[Downloaded from stdc.iust.ac.ir on 2025-07-19]

[DOI: 10.22068/ijmse.2266]

segregated phases were eliminated from the microstructure by a 15-hour solution treatment, some phases with low melting points could once again form during the pre-heating in the hot rolling process. On the other hand, the Sn-rich phase containing 43%wt Sn (region A in Fig. 2 (b)) segregates at the microstructure which might be a multi-component phase with a low melting temperature. Interestingly, our experiments showed that approximately similar results could be achieved by the warm rolling of the alloy at a temperature range between 200-500°C. As mentioned before standard warm tension test was performed at 670°C to make sure that the poor workability which was observed is not affected by the rolling processing parameters. The result confirmed that re-segregation of second phases after pre-heating reduces the formability of alloy which is the reason for the failure of high temperature rolling processes.

4. CONCLUSIONS

- The segregated phases rich in Sn, Mn, Ni, and Fe in the microstructure of the PM-17 alloy causes the formation of cracks during the rolling process.
- Solution treatment at 750°C for 15 hours was applied in order to eliminate the formation of segregated phases and to reduce Brass and Goss-textures in the specimen. This is the only way to roll the alloy into small thicknesses.
- By applying solution treatment, the amounts of MTR and MRPRP compared with the as-cast samples increased from 16.37 and 8.19 to 109.46 and 15.64, respectively. However, due to the re-formation of the low melting temperature phases, proper hot rolling was not possible even for the solution-treated samples.

REFERENCES

[1] Schwartz, M. M., Brazing, Second Edition, Chapter 3, Elements of the Brazing Process, ASM international, Material Park Ohio, 2003, 15-59.

[2] Cai, C., Lumpp, J.K., "Microstructural studies of Cu brazing on AlN." J. Mater. Res., 2001, 16, 670–677, https://doi.org/10.1557/JMR.2001.0125.

[3] R. K. Roy, A. Panda, S. K. Das and A. Mitra, "Development of a copper-based filler alloy for brazing stainless steels." Mater. Sci. Eng., A, 2009, 523, 312-315. https://doi.org/10.1016/j.msea.2009.05.049.

[4] Pashkov, A., Gerasimov, S., and Pashkov, I., "Special features of brazing of the copper–manganese–nickel system with a powder brazing alloy." Welding International, 2010, 24, 5, 385-389.

[5] Yu, Z. S., Qian, Y. Y., Li, R. F., and Zhou, F. M., "Surface wetting and interfacial behaviour in arc brazing of titanium alloy." Mater. Sci. Technol., 2003, 19, 1399-1402.

[6] Chatterjee, S., Mingxi, Z. and Chilton, A., "The Development of New Silver-Free Brazing Alloys for Steel Tubular Assembly." Welding journal, 2002, 71, 149-155.

[7] Zheng, Y., Li, N., Yan, J. and Cao, Y., "The microstructure and mechanical properties of 1Cr17Ni2/QAl7 brazed joints using Cu-Mn-Ni-Ag brazing alloy." Mater. Sci. Eng., A, 2016, 661, 25-31.

[8] Venkateswaran, T., Thinesh, T. B., Agilan, M., Sivakumar, D., Pant, B. and Sudhakar, D., "Optimization and Characterization of Manganese Coating on Cu-Cr-Zr-Ti Alloy." Mater. Sci. Forum, 2015,830, 671-674.

[9] Suslov, A., "Brazing in gas media three-layer structures of high-strength steels." Weld. international, 1998, 12, 12, 1000-1002.

[10] Kalinin, G., Krestnikov N., Jarovinskiy, Y. L., Makhin, I., Nikolaev, V., Skladnov, K., Strebkov, Y. S., and Zolotarev, V., "Microstructure investigation of bronze/steel brazed joints proposed for HHF components of ITER manufacturing." Fusion Eng. Des., 2008, 83, 10, 1521-1523.

[11] Imaev, R.M., Imaev, V.M. & Khismatullin, T.G., "Refining of the microstructure of cast intermetallic alloy Ti- 43% Al-X (Nb, Mo, B) with the help of heat treatment." Met. Sci. Heat Treat., 2006, 48, 81–84. https://doi.org/10.1007/s11041-006-0048-4R.

[12] Jiang, P., Yu, Y., Song, G., Liang, D., Kellam, M., and Dolan, M., "Effect of heat treatment on microstructure,

[Downloaded from stdc.iust.ac.ir on 2025-07-19]

[DOI: 10.22068/ijmse.2266]

hardness and rollability of $V_{55}Ti_{30}Ni_{15}$ alloy membranes." Mater. Des., 2014, 63, 136-141.
[13] Li, W., Zhou, H. and Li, Z., "Effect of gadolinium on microstructure and rolling capability of AZ31 alloy." J. Alloys Compd., 2009, 475, 227-232.
[14] Zou, J., Yan, H., Chen, J., Xia, W., Su, B., Lei, Y. and Wu, Q., "Effects of Sn on microstructure and mechanical properties of as-rolled Mg–5Zn–1Mn alloy." Mater. Sci. Technol., 2018, 34, 1468-1479.
[15] Zhu, Y. Z., Huang, R. Y., Zhu, Z. and Xiang, Z. D., "Comparative study on effects of microstructures of hot rolled and twin roll casting 1235 aluminium alloy on surface quality of aluminium foils produced." Mater. Sci. Technol., 2011, 27, 761-766.
[16] Foulger, R. V. and Nicholls, E., "Influence of composition and microstructure on mechanical working properties of copper-base alloys." Metals Tech., 1976, 3, 366-369.
[17] Korneva, A., Straumal, B., Chulist, R., Kilmametov, A., Bata, P., Cios, G., Schell, N. and Zięba, P., "Grain refinement of intermetallic compounds in the Cu–Sn system under high pressure torsion." Mater. Lett., 2016, 179, 12-15.
[18] Bayle, B., Bocher, P., Jonas, J. J., and Montheillet, F.," Flow stress and recrystallisation during hot deformation of Cu–9%Sn alloys." Mater. Sci. Technol., 1999, 15, 803-811.
[19] Peng, G., Gan, X., Jiang, Y., Li, Z. and Zhou, K., "Effect of dynamic strain aging on the deformation behavior and microstructure of Cu-15Ni-8Sn alloy." J. Alloys Compd., 2017, 718, 182-187.
[20] Virtanen, P. and Tiainen, T., "Stress relaxation behaviour in bending of high strength copper alloys in the Cu–Ni–Sn system." Mater. Sci. Eng., A, 1997, 238, 2, 407-410.
[21] Neishi, K., Uchida, T., Yamauchi, A., Nakamura, K., Horita, Z. and Langdon, T., "Low-temperature superplasticity in a Cu-Zn-Sn alloy processed by severe plastic deformation." Mater. Sci. Eng., A, 2001, 307, 1, 23-28.
[22] Sadeghi, Mohammadi, M., Hadi, M., Karimi, H. and Bayat, O., "Determination Of Critical Pressure And Impeding Pressure For Manganese Evaporation During The Induction Melting Process Of Manganese-Nickel Alloys." Founding Res. J., 2019, 3, 67-74.
[23] Hadi, M., Kamali, A., Khalil, J. A, Ebrahimi, A. and Hadavi, M., "Elimination of inclusions and evaporation control during melting of Ti-48Al-2Cr-2Nb-1B intermetallic alloy." Russ. J. Nonferrous Met., 2009, 50, 24-29.
[24] Kamali, A. R., Hadi, M. and Nazarian-Samani, M., "Two different methods for improving the properties of IC-221M alloy." IJEMS, 2009, 16, 6, 449-455.
[25] Kim, S.H., Han, S. Z., Kim, C. J., Hwang, I.Y. and Yin, F., "Evolution of Rolling Textures of Cold Rolled Copper Foils." Mater. Trans., 2009, 50, 3, 537-543.
[26] Kestens, L., and Pirgazi, H., "Texture formation in metal alloys with cubic crystal structures." Mater. Sci. Technol., 2016, 32, 13, 1303-1315.
[27] Yan, H., Zhao, X., Jia, N., Zheng, Y. and He, T., "Influence of Shear Banding on the Formation of Brass-type Textures in Polycrystalline fcc Metals with Low Stacking Fault Energy." J. Mater. Sci. Technol., 2014, 30, 408-416.
[28] Geng, Y., Ban, Y., Wang, B., Li, X., Song, K., Zhang, Y., Jia, Y., Tian, B., Liu, Y. and Volinsky, A. A., "A review of microstructure and texture evolution with nanoscale precipitates for copper alloys." J. Mater. Res. Technol., 2020, 9, 11918-11934.
[29] Zhao, Y., Zhang, H., Fan, J., Wang, L., Zhang, Q., Peng, C., Dong, H. and Xu, B., "Grain refining and improving mechanical properties of AZ31 Mg alloy sheets by multi-pass warm rolling with falling temperature." J. Mater. Res., 2018, 33, 2827-2834.
[30] Huang, X., Suzuki, K., Watazu, A., Shigematsu, I. and Saito, N., "Effects of manganese addition on microstructure and press formability of hot-rolled Mg–Al–Zn alloy sheets." J. Mater. Res., 2008, 23, 3029-3039.
[31] Liu, Z., Chen, Y., Wei, H. and Li, Z., "Study on the distribution of texture and

[Downloaded from stdc.iust.ac.ir on 2025-07-19]

[DOI: 10.22068/ijmse.2266]

the second phase under different aging process of Cu-Ni-Si alloy." Mater. Lett., 2019, 236, 292-294.
[32] Fei, W., Li, Z. and Li, Y., "Effects of T4 treatment on hot rolling behavior and tensile strength of aluminum matrix composite reinforced by aluminum borate whisker with NiO coating." Mater. Chem. Phys., 2006, 97, 402-409.
[33] Kang, Z. X., Lin, K. and Zhang, J. Y., "Characterisation of Mg–Li alloy processed by solution treatment and large strain rolling." Mater. Sci. Technol., 2016, 32, 498-506.
[34] Baker, T. N., and Mcpherson, N. A., "Effect of solution temperature and rolling schedule on niob, ium steel controlled-rolled into ferrite temperature rang." Met. Sci., 1997, 13, 11, 611-618.
[35] Dai, Q., Lan, W. and Chen, X., "Effect of Initial Texture on Rollability of Mg-3Al-1Zn Alloy Sheet." J. Eng. Mater. Technol., 2014, 136, 110-115.
[36] Wang, J.Y., Saufan, A., Lin, P., Bor, H., Lee, S. and Kawamura, Y., "Mechanical properties and strengthening behavior of Mg–Zn–MM alloy." Mater. Chem. Phys., 2014, 148, 28-31.
[37] Hadi, M., Meratian, M. and Shafyei, A., "The effect of lanthanum on the microstructure and high temperature mechanical properties of a beta-solidifying TiAl alloy." J. Alloys Compd., 2015, 618, 27-32.
[38] Hadi, M., Shafyei, A. and Meratian, M., "A comparative study of microstructure and high temperature mechanical properties of a β-stabilized TiAl alloy modified by lanthanum and erbium." Mater. Sci. Eng., A, 2015, 624, 1-8.
[39] Hadi, M., and Kamali, A. R., "Investigation on hot workability and mechanical properties of modified IC-221M alloy." J. Alloys Compd., 2009, 485, 204-208.

[Downloaded from stdc.iust.ac.ir on 2025-07-19]

[DOI: 10.22068/ijmse.2266]